A New Model for Generating Mass-Consistent Wind Fields Over Continuous Terrain

S.T. Chan

G. Sugiyama

November 1996

A NEW MODEL FOR GENERATING MASS-CONSISTENT WIND FIELDS OVER CONTINUOUS TERRAIN

Stevens T. Chan
Lawrence Livermore National Laboratory
P.O. Box 808, L-103
Livermore, CA 94550
(510) 422-1822

Gayle Sugiyama
Lawrence Livermore National Laboratory
P.O. Box 808, L-103
Livermore, CA 94550
(510) 422-7266

SUMMARY

Based on a mixed variational principle and the finite element method, a model for efficiently generating mass-consistent wind fields over continuous terrain has been developed. Two numerical examples are presented to demonstrate the applicability of the model.

I. INTRODUCTION

As part of the modernization efforts of the Atmospheric Release Advisory Capability (ARAC) project, we have developed a new diagnostic model for generating mass-consistent wind fields over continuous terrain. Such wind fields can be used to drive ARAC's new dispersion model LODI[1]. This model is going to replace our current operational code MATHEW[2], which uses stair-step topography and constant grid spacings.

Our new model is based on a mixed variational principle and the finite element method (FEM) for spatial discretization. Two conjugate gradient solvers are implemented for efficiently solving the Poisson equation resulting from the numerical formulation. The finite element method is employed to effectively treat continuous terrain and variable grid resolution. It is based on a grid-point representation of the wind fields in contrast to the flux-based, staggered grid representation often used in finite difference approaches. Additionally, the model offers a very flexible treatment of boundary conditions and the ability to preserve velocity at desired grid-points for cells in which wind observations are located. Also included in our model are map projection factors and differential weighting for the horizontal and vertical velocity adjustments to reflect the effects of atmospheric stability.

II. NUMERICAL MODEL

A. Governing Equations

The underlying theoretical basis of our model, with the assumption of constant density, is the following functional,

$$I(u,v,w;\lambda) = \frac{1}{2}\int\left[\alpha_H^2\left(u-\tilde{u}\right)^2 + \alpha_H^2\left(v-\tilde{v}\right)^2 + \alpha_v^2\left(w-\tilde{w}\right)^2\right]d\Omega + \int\lambda\left(\frac{\partial u}{\partial x}+\frac{\partial v}{\partial y}+\frac{\partial w}{\partial z}\right)d\Omega \qquad (1)$$

In the above equation, $(\tilde{u},\tilde{v},\tilde{w})$ and (u, v, w) are the components of the initial and adjusted velocity fields, λ is the Lagrange multiplier, α_H and α_v are the Gauss precision moduli, and Ω is the domain under consideration. Equation (1) is a mixed variational principle[3] for which the solution $(u, v, w; \lambda)$ is a saddle point, rather than an extremum point. The solution corresponds to a minimum with respect to the difference between the adjusted and the initial velocity fields and a maximum with respect to the Lagrange multiplier. With this approach, the mass-conservation requirement will be enforced as a strong constraint.

It can be shown that the solution of (1) via taking $\delta I = 0$ leads to the following Euler-Lagrange equations,

$$u = \tilde{u} + \frac{1}{\alpha_H^2}\frac{\partial\lambda}{\partial x} \qquad (2a)$$

$$v = \tilde{v} + \frac{1}{\alpha_H^2}\frac{\partial\lambda}{\partial y} \qquad (2b)$$

$$w = \tilde{w} + \frac{1}{\alpha_v^2}\frac{\partial\lambda}{\partial z} \qquad (2c)$$

$$\frac{\partial u}{\partial x}+\frac{\partial v}{\partial y}+\frac{\partial w}{\partial z} = 0 \qquad (3)$$

in Ω, and

$$\lambda \delta u_n = 0 \qquad (4)$$

on the boundary. In equation (4), δu_n is the first variation of the adjusted velocity in the normal direction. This equation implies that, on the boundary, either

$$\delta u_n = 0 \text{ or } \lambda = 0.$$

The former corresponds to a boundary where the normal velocity is specified, such as $u_n = \bar{u}_n$ on an inflow plane or $u_n = 0$ on a solid boundary, while the latter corresponds to "flow through" boundaries (which is a natural boundary condition for the velocity).

B. Finite Element Discretization

The FEM with piecewise polynomial basis functions is used for spatial discretization of (1). Specifically trilinear functions defined on a general hexahedron are used for the velocity and piecewise constants are used for the field of Lagrange multiplier. Upon using the above approximations and setting $\delta I = 0$, a coupled system of algebraic equations is obtained,

$$MU + C\lambda = M\tilde{U} \qquad (5)$$

and

$$C^T U = 0 \qquad (6)$$

In the above equations, U is a vector containing all the nodal values of (u, v, w), $\tilde{U}$ is a vector for $(\tilde{u}, \tilde{v}, \tilde{w})$, and λ is a vector for the Lagrange multiplier of all elements. M is the mass matrix of size 3n x 3n, C is the gradient matrix of size 3n x m, and C^T, the transpose of C, is the divergence matrix. There are n nodes for the velocity and m elements for λ. Alternatively, equations (5) and (6) could be obtained by applying the Galerkin method of weighted residuals to (2) and (3) and integrating by parts the terms involving λ.

Equations (5) and (6) could, in principle, be solved as a coupled system. However, such an approach may prove impractical for large problems, due to excessive memory and CPU requirements. We implemented a cost-effective alternative developed by Gresho et al.[4], which uses, in place of the original consistent mass matrix, a lumped (via row-sum) mass matrix (denoted below as M_L), and solves the following equivalent uncoupled system,

$$\left(C^T M_L^{-1} C\right)\lambda = C^T \tilde{U} \qquad (7)$$

and

$$U = \tilde{U} - M_L^{-1} C\lambda \qquad (8)$$

To efficiently solve large linear systems of equations such as (7), we use the incomplete Cholesky-conjugate gradient (ICCG) method of Kershaw[5] and the diagonally scaled conjugate gradient (DSCG) method.

C. Treatment of Terrain

One of the advantages of the finite element method is that all calculations are carried out directly in the physical space of (x, y, z), although our input/output data are associated with the (x, y, σ_z) coordinate system. Such an approach can save computational time and, more importantly, guarantees that the resulting wind field is mass-consistent in the physical space. To impose the boundary condition of no-penetration on the ground surface, local transformation matrices of size 3 x 3, which relate the Cartesian velocity components to those in the local normal/tangential directions, are first evaluated for all nodes on the terrain surface. These transformation matrices, defined by the direction cosines of the consistent normal direction derived by Engleman et al.[6], are then incorporated into the global gradient and divergence matrices (C and C^T), thus allowing a direct computation of velocity components in the local normal/tangential directions and the specification of zero normal velocity component on the ground surface.

III. NUMERICAL EXAMPLES

A. Flow Around a Hemispheric Hill

To test the accuracy of our model, we calculated the potential flow around a hemispheric hill. The analytic solution for this problem, in terms of the velocity potential function, is

$$\Phi = u_o x\left(1 + r_o^3 / 2r^3\right), \quad r \geq r_o \qquad (9)$$

in which u_o is the free stream velocity and r_o is the radius of the hill. The velocity components corresponding to (9) are

$$u = u_o\left[1 + \left(y^2 + z^2 - 2x^2\right)r_o^3 / 2r^5\right]$$
$$v = -3u_o xy r_o^3 / 2r^5 \qquad (10)$$
$$w = -3u_o xz r_o^3 / 2r^5$$

In the numerical simulation, a hemispheric hill of radius 1 km was placed in the center of a computational domain of 5km x 5km x 2km in the downwind, crosswind, and vertical directions, respectively. The computational mesh (or grid) consists of 50 x 50 x 30 elements (or zones) and the mesh is basically uniform in the two horizontal directions and gradually graded in the vertical direction, with finer zones near the ground. To account for the

relatively short distance from the inflow plane to the hill, exact velocity components as defined in (10) were specified on that plane. No-penetration was imposed along the terrain surface and the 'flow-through' boundary condition was assumed on all the remaining boundaries. A uniform wind of $u_o=1$ m/s was used as the initial guess. The entire simulation took 26 sec on a DEC Alpha machine.

In Fig. 1, mass-consistent velocity vectors on the center plane and the 100-m horizontal plane are displayed. The wind field exhibits the stagnation points at the front and the rear of the hill and shows the potential flow following the surface of the hill. The predicted maximum speed at the peak of the hill is 1.56 m/s, versus the theoretical value of 1.50 m/s.
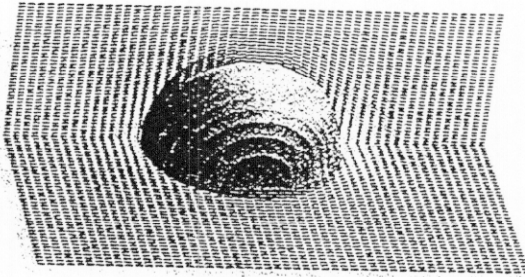

Fig. 1. Predicted velocity vectors on z = 100 m and the center planes

The 0.15 m/s speed deviation contour (which corresponds to 10% of the theoretical maximum speed) from the exact solution is shown in Fig. 2. Most of the computational domain has speed deviations less than 0.15 m/s, but larger errors exist near the lower part of the hemisphere. Greater errors are naturally expected in this region, because the mesh resolution is relatively coarse to resolve the steepest slopes there. The overall accuracy of
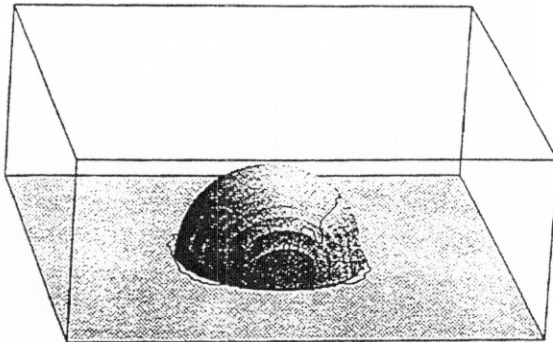

Fig. 2. The contour of 0.15 m/s speed deviation from exact solution

the solution is much higher; the root-mean-square error of the speed deviations for the entire domain is only 0.032 m/s.

B. Application for the San Francisco Bay Area

In this example, our model is applied to generate the wind fields for an emergency response scenario in the San Francisco Bay Area, using interpolated wind data from the new ARAC meteorological database (see Sugiyama and Chan[7]). The grid is 100 km by 100 km by 3 km, with 81 grid points in each horizontal direction and 31 grid points in the vertical direction. The grid has 10 m vertical resolution near the ground. The entire simulation took 87 sec on a DEC Alpha machine.

Fig. 3 shows the mass-consistent wind vectors on the 10 m AGL plane, together with the surface observations (plotted within the circles). In general, only small changes were made to the initial winds by the mass-adjustment model. In Fig. 4, wind vectors on the y-z plane in the middle of the grid are shown, with the vertical wind components scaled by a factor of 10. The variable grid employed and the terrain following adjusted velocity vectors can be seen in this figure. The magnitude of the vertical wind induced by the topography is not very large, which is consistent with the small changes observed above for the horizontal winds.
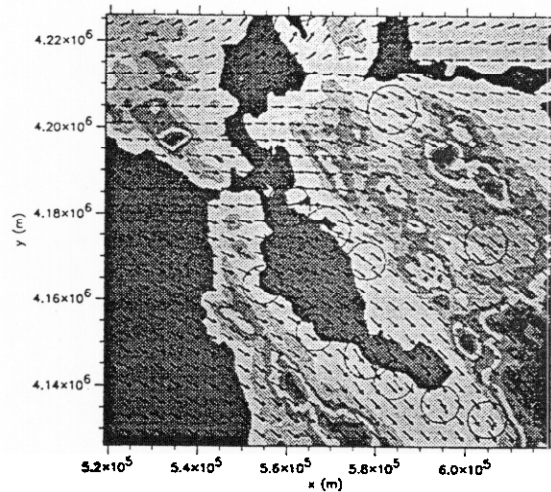

Fig. 3. Mass-consistent surface wind filed at 10 m AGL. Every third vector is plotted. Surface wind observations are plotted within the circles.
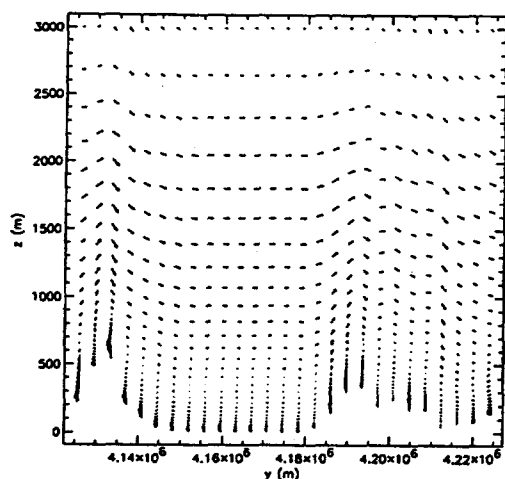
Fig. 4. Wind vectors on the cross wind plane at x = 570 km

IV. CONCLUSION

A new model based on a mixed variational principle and the FEM has been developed for efficiently generating mass-consistent wind field over continuous terrain. Results from our early testing and applications indicate that the model is robust and sufficiently fast for real-time assessment purposes. The model will be further evaluated in practical applications using measured data and forecast fields. Additional physics and parameterizations, including spatial variations of the Gauss precision moduli depending on atmospheric and topographical conditions, will be implemented in the near future.

ACKNOWLEDGMENTS

REFERENCES

1. J. M. Leone, Jr., J. S. Nasstrom, and D. Maddix, "A First Look at the New ARAC Dispersion Model," ANS 6th Topical Meeting on Emergency Preparedness and Response, San Francisco, CA (1997).

2. C. A. Sherman, "A Mass-Consistent Model for Wind Fields Over Complex Terrain," *J. Appl. Meteor*, 17, 312-319 (1978).

3. D. N. Arnold, "Mixed Finite Element Methods for Elliptic Problems," *Comput. Methods Appl. Mech. Engrg.* 82, 281-300 (1990).

4. P. M. Gresho, S. T. Chan, C. D. Upson, R. L. Lee, "A Modified Finite Element Method for Solving the Time-Dependent, Incompressible Navier-Stokes Equations," *Int. J. Num. Meth. Fluids*, 4, 557-598 & 619-640 (1984).

5. D. Kershaw, "The Incomplete Cholesky-Conjugate Gradient Method for the Iterative Solution of Systems of Linear Equations," *J. Comp. Phys.*, 26, 43-65 (1978).

6. M. S. Engleman, R. L. Sani, and P. M. Gresho, "The Implementation of Normal and/or Tangential Boundary Conditions in Finite Element Codes for Incompressible Fluid Flow," *Int. J. Num. Meth. Fluids*, 2, 225-238 (1982).

7. G. Sugiyama and S. T. Chan, "Meterological Data Assimilation for Real-Time Emergency Response," ANS 6th Topical Meeting on Emergency Preparedness and Response, San Francisco, CA (1997).